doi: 10.5937/SimTerm24374K

Influence of Building Shape on Wind Flow: CFD simulations

Danka Kostadinović[a], Ivan Lazović[a]

[a]University of Belgrade, Vinča Institute of Nuclear Sciences-National Institute of the Republic of Serbia, Department of Thermal Engineering and Energy, Belgrade, ISO 3166-1:RS, dankak@vin.bg.ac.rs

Abstract: Buildings significantly affect the wind flow pattern over an urban area, leading to regions with an accelerated wind flow. The change in wind flow influences pollutant dispersion, urban microclimate, formation of fog and haze, urban heat island, comfort of pedestrians, and wind-created noise. It is important to include the simulation of wind flow around buildings in the early architectural design stage. The paper investigates the effect of different shapes of buildings on the wind flow pattern using Computational Fluid Dynamics (CFD) simulation. Results have been represented through pressure, velocity, and turbulence kinetic energy contours for five different cases. The ANSYS software was employed to solve the flow governing equations. The standard k-ε turbulent model was used for turbulence modeling while the Semi-Implicit Method for Pressure Linked Equation (SIMPLE) algorithm was applied as a solver for governing equations. This study clearly illustrates that different building shapes generate different wind flow patterns.

Keywords: ANSYS, Building, CFD, Turbulence, Velocity, Wind.

1. Introduction

Urbanization is one of the major driving forces behind the expansion of cities and the increase in built density. The wind flow around buildings in an urban area is an important consideration in the design of building layouts, natural ventilation design, air pollutant dispersion, and pedestrian comfort [1], [2]. The roughness of the ground surface affects the flow of air immediately above the terrain. In the atmospheric boundary layer, the wind speed changes from zero near the ground due to the no-slip condition to some constant value at a certain distance from the ground where surface friction has a negligible effect on wind speed. Within the boundary layer, the wind is turbulent with sudden changes in direction and speed due to the earth surface itself such as roughness, and friction. The wind speed increases with the distance from the ground, so high-rise buildings are exposed to stronger wind. The boundary-layer flow of the atmosphere affects the urban climate, urban heat island, and formation of fog and haze [3]. Wind flow around buildings is dependent on building density [4], while the arrangement and height of buildings affect urban ventilation [5], [6].

There is a large number of high-rise buildings constructed in developed countries. Taller and taller structures are being designed which have a significant effect on the surrounding wind pattern. Buildings change not only the direction of the wind but also change its speed. In the cities, the wind speed is reduced by 25-30%. Buildings produce air pollution in the form of exhaust from heating systems (fossil fuel boilers), kitchens, and smoking. Sourinding of buildings also experience air pollution from traffic. The wind flow around the buildings influences on dispersion of pollutants and the exposure of people to air pollution near the buildings. The distribution of pressure on the building and structural load is related to the wind flow around them. Strong winds can cause damage to buildings, therefore to prevent structural failures it is necessary to determine the wind load on buildings. The wind flow near a building affects the surface movement of rain as well as the performance of heating, cooling, and ventilating systems.

The change in wind speed at the pedestrian level influences on comfort of people near the building. Classification of wind speed and human body feeling, based on [7] is given in Table 1. At pedestrian level, a wind of 10 m/s is considered to be intolerable and disagreeable, while wind of 5 m/s is considered to be annoying [8]. Wind speed ranging from 1 m/s to 5 m/s is the most comfortable for humans. Pedestrian comfort needs to be considered during building design and city planning. Improving the structure of urban areas can improve the wind flow and environmental conditions. Consequently, the architect and planner need to predict the wind flow near buildings, and related aspects of its performance. The wind flow around buildings can be investigated from field experiments, in wind tunnel tests under strictly controlled conditions, and simulations based on Computational Fluid Dynamics (CFD). Field experiments give more realistic parameters, however the testing period time-consuming, and require a lot of material resources and labor. Wind tunnel experiments are complex, time-consuming, and very expensive. Instead, CFD simulations are used. CFD models avoid the impacts of walls in wind tunnels, and allow simulations of objects with real scale dimensions and quick change of geometrical design and boundary conditions to analyze the influence of an individual parameter. The CFD simulations of wind flow in urban areas can be classified into three categories: full-scale models, mesoscale models, and individual buildings. The building configurations can be categorized into building complexes, street canyons, and isolated buildings. Previous review studies related to wind flow assessment have been published focused on the velocity measurement techniques [9], wind flow in street canyon [10], air quality and pollutant dispersion [11], [12], while study [13] reviewed wind tunnel and CFD techniques. Wind flow patterns around isolated buildings are crucial for a deep understanding of wind flow patterns around complex building layouts. Characteristics of wind flow around buildings with different shapes predicted by CFD simulation are discussed in this paper. This research is based on the following questions: What is the change in pattern of wind, pressure, and turbulence kinetic energy with the change of building's shape? The Ansys software was used to simulate the flow of wind around a building. This study highlights the role of urban physics characteristics on wind flow.

2. Methodology

Using CFD simulations, the impact of buildings on wind flow is examined. The process to obtain wind paterns may be divided into five main steps: model geometry, model meshing, setup boundary conditions, solution, and results.

2.1. Computational Domain and Mesh

Previous studies revealed that 2-D simulation encountered inaccurate prediction of wind pressure on the building [14], thus 3-D models were used in the present study. A three-dimensional rectangular computational domain with relevant distances, shown in Figure 1, is considered for modeling wind flow around the building. The dimensions of the computational domain were selected based on the study [15]. To ensure the full development of turbulent flow the computational domain was set as 5H upstream and 15H downstream, where H is the building height. The length of the domain behind the building is greater than the length from the inlet to to building due to reestablishing a uniform flow of airflow behind the building. From the top of the building to the upper boundary of the domain, the distance should be sufficient to prevent the occurrence of artificially induced acceleration in this zone. The computational geometry in the software is modeled at scale 1:1. Each building is regarded as rigid or non-deformable.

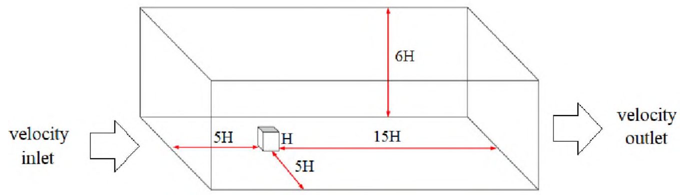

Figure 1. Computational domain with relevant distances

Simulation and result accuracy depend upon mesh quality. A finer mesh will yield more accurate results as it divides the volume around the model into smaller volumes, however, it increases the computing time. The meshing of the CFD domain and building model is presented in Figure 2. A structural tetrahedral grid was used for meshing. The finer mesh was used around the building to capture more details of the flow parameters near the envelopes of the building. Since the computational time required for the simulation larger elements were applied to the domain far from the building. It was considered that convergence is ensuring if the residual fell below the generally applied criteria of dropping to 10−4. It was also necessary to create names for all external surfaces on which the boundary conditions would be later defined. For surfaces that have the same name, the same boundary conditions are set.

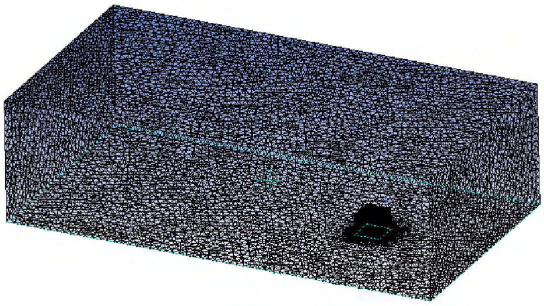

Figure 2. Grid used for three-dimensional representation of the cubic low-rise building

2.2. Governing equations

The Ansys Student Version 18.1 software [16], which is based on the finite volume method, was used to numerically solve the following partial differential equations: equation of continuity and momentum equations (Reynolds averaged Navier-Stokes - RANS) equation.

$$\frac{\partial \bar{v_i}}{\partial x_i} = 0 \quad (1)$$

$$\rho\left(\frac{\partial \bar{v_i}}{\partial t} + \bar{v_j}\frac{\partial \bar{v_i}}{\partial x_j}\right) = \rho \bar{F_i} - \frac{\partial \bar{p}}{\partial x_i} + \frac{\partial}{\partial x_j}\left(\eta \frac{\partial \bar{v_i}}{\partial x_j} - \rho \overline{v_i' v_j'}\right) \quad (2)$$

Previous studies examined the application of different turbulence models for the simulation of wind flow [17], [18]. It is noticeable that the k-ε model [19], also known as the Launder Spalding model, is the most commonly used engineering model for turbulence flow. The standard K-ε turbulence model was used in this research to address the simulation of wind flow. In this model, it is considered that the flow is completely turbulent, and the effect of molecular viscosity is negligible. Two supplementary transport equations are needed for the turbulence kinetic energy and its dissipation.

$$\left(\frac{\partial k}{\partial t} + \bar{v_j}\frac{\partial k}{\partial x_j}\right) = P - \rho\varepsilon + \frac{\partial}{\partial x_j}\left(\left(\eta + \frac{\eta_t}{\sigma_k}\right)\frac{\partial k}{\partial x_j}\right) \quad (3)$$

$$\rho\left(\frac{\partial \varepsilon}{\partial t} + \bar{v_j}\frac{\partial \varepsilon}{\partial x_j}\right) = \frac{\partial}{\partial x_j}\left(\left(\eta + \frac{\eta_t}{\sigma_\varepsilon}\right)\frac{\partial \varepsilon}{\partial x_j}\right) + C_{\varepsilon 1}\frac{\varepsilon}{k}P - \rho C_{\varepsilon 2}\frac{\varepsilon^2}{k} \quad (4)$$

The term of the connection of Reynolds stress and gradient of the mean field represents the production of turbulent energy.

$$P = -\rho \overline{v_i' v_j'}\frac{\partial \bar{v_i}}{\partial x_j} \quad (5)$$

Several empirically determined constants appear in the equations which have the following values when performing numerical simulations of wind flow:

$$C_\eta = 0.09 \quad C_{\varepsilon 1} = 1.44 \quad C_{\varepsilon 2} = 1.92 \quad \sigma_k = 1 \quad \sigma_\varepsilon = 1.3 \quad (6)$$

Pressure-velocity coupling is taken care of by the SIMPLE algorithm.

2.3. Boundary conditions

Boundary conditions that simulate the actual flow are necessary for the real physical demonstration of the airflow. The following types of boundary conditions were used:

- wind speed on the upstream side of the building at thedomain inlet,
- pressure equal to atmospheric on the outlet downstream side,
- boundary condition on the wall.

At the inlet to the domain, a constant wind speed was set along the height. The wind speed wasn't the same in every case study. A wind direction is orthogonal to the observed domain. A pressure equal to atmospheric is set at the outlet of the domain. At all the sides of the building, the nonslip wall conditions were applied. The air temperature at the inlet and outlet of the domain is 26 °C, while the intensity of turbulence is 5%. The solution is initialized with the values of the input boundary conditions. The no-slip wall condition is used for the building and ground surface.

3. Results

Wind flow around the cube, high-rise, L-shaped, and cylindrical building with an orientation normal to the incident wind flow was simulated. The pressure contours around buildings in a horizontal plane are shown in Figure 3. The horizontal plane is positioned at half of the building's height. The first case that was considered is the flow of wind with a speed of 5 m/s around an isolated cube building with dimensions of 10x10x10 m. The height of the L-shaped building is 15 m while the wind speed is 10 m/s. The isolated high-rise building has dimensions of 30x30x80 m and wind speed of 25 m/s. The cylindrical building has a diameter of 50 m and a height of 40 m while the wind speed is 10 m/s. In all observed cases, the positive pressure is on the upstream side of the building as a result of the wind hitting the windward side. A stagnation point with the highest pressure is at approximately two-thirds of the building height. The negative pressure is attained on the top face, lateral sides, and leeward sides due to flow separation. The pressure on the leeward sides is lower than the pressure on the leeward side, except in the case of high-rise building. Pressure increases from the edges to the center on the windward side, while on the leeward side, pressure decreases from top to bottom. In the case of L shape building, two stagnation points can be observed on the upstream side of the building. The underpressure zone on the downstream side of the building is much larger than in the other cases. Around the high-rise building, the concern of the wind flow is greater, as is the height of the building, so the overpressure zone on the windward as well as the underpressure on the leeward sides of the building are larger. The L-shaped and high-rise buildings have a larger zone of negative pressure on the leeward side than the cube and cylindrical buildings. In the case of cylindrical building positive pressure on the leeward side is obtained. Underpressure zones exist only on the latreal sides.

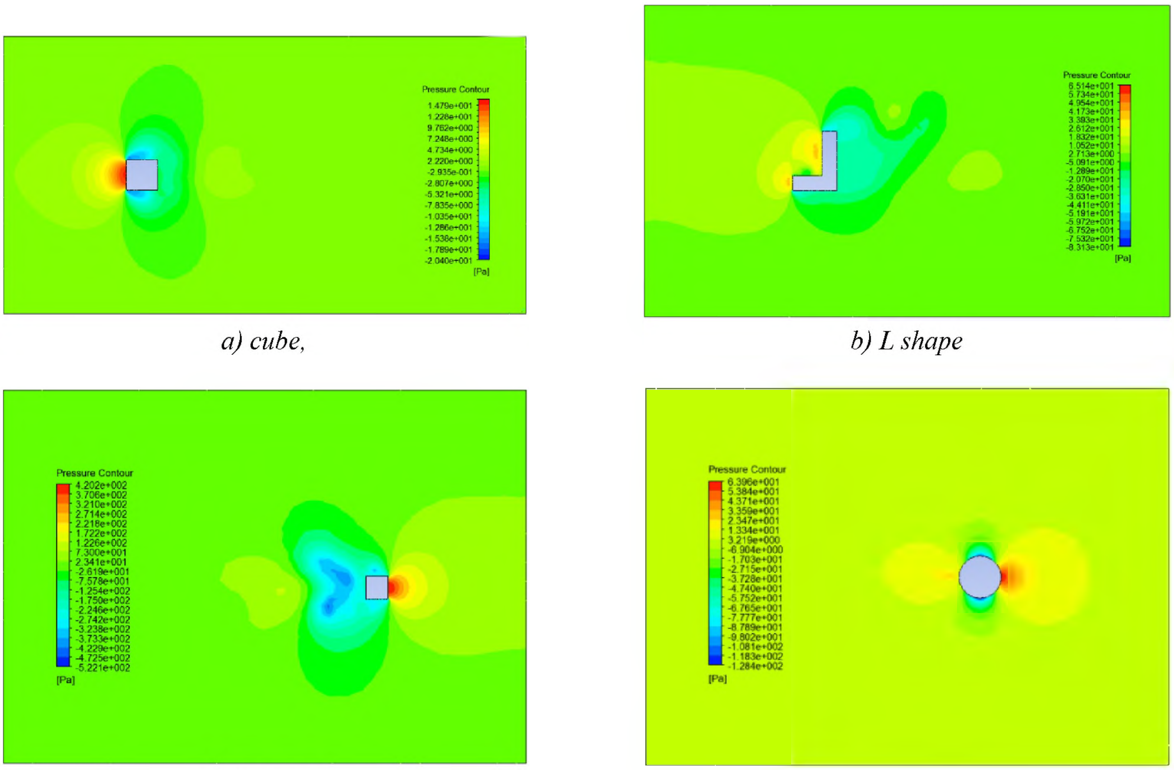

a) cube, *b) L shape*

c) high rise *d) cylindrical building*

Figure 3. Pressure contours around a) cube, b) L shape, c) high rise, d) cylindrical building

The velocity contours around buildings in a horizontal plane are shown in Figure 4. Generally, the flow separation occurs at the lateral sides of the buildings where maximum wind velocity can be noticed (red area in Figure 4). In all observed cases, the zones of increased wind speed can be observed on the lateral sides of buildings. There is a large velocity gradient in these positions and underpressure zones. The velocity gradient is lowest in the case of cylindrical building. The velocity contours in the horizontal plane clearly show the existence of a turbulent zone on the leeward side. The overall flow patterns show more substantial disturbance on the leeward side than on the windward side. The wind reaches the undisturbed field far away from the building. The wider building disturbs a longer and wider region on the windward and leeward side of the building. The non-symmetrical L shape of the building causes the non-symmetrical distribution of velocity contours around the building in the horizontal plane. For an L-shaped building with the larger wide, the wind flow deflecting towards the lateral sides travels a longer distance towards the flow detachment at the windward side of the building. Therefore, frictional effects exist over a longer distance and dissipate higher amounts of kinetic energy of the wind resulting in lower wind velocity around the lateral sides. The wider L-shaped building causes the formation of a longer recirculation region on the downstream side of the building. In the case of cylindrical building, the wind flow is least disturbed.

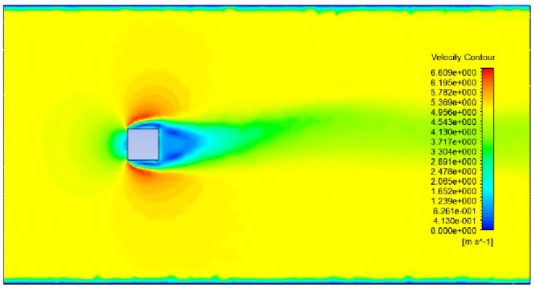

a) cube,

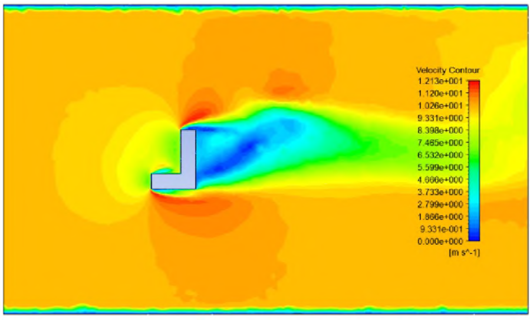

b) L shape

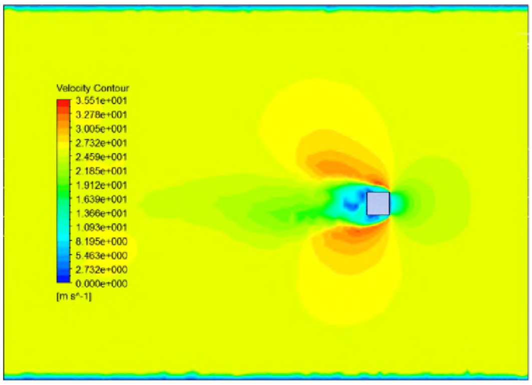

c) high rise

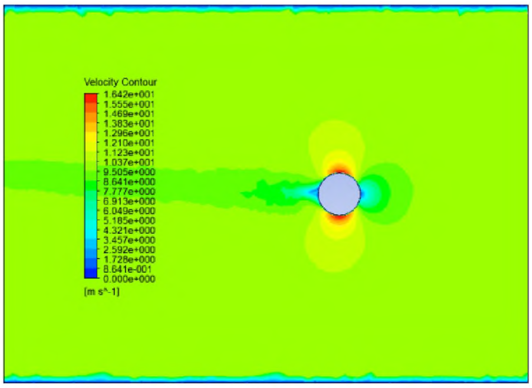

d) cylindrical building

Figure 4. Velocity contours in horizontal plane around a) cube, b) L shape, c) high rise, d) cylindrical building

The velocity contours around buildings in the vertical plane are shown in Figure 5. The vertical plane is positioned at half of the domain width. The wind velocity around the upwind edges and the lateral sides of the building increases with increasing building height. The wind velocity is highest at the upwind edges on the windward face of the high-rise building. Figure 4 and Figure 5 clearly show that at the top of the buildings and their lateral sides wind flow is detached from the surface and flow separation takes place. The separation bubbles are formed in these places characterized by reverse flows, low-velocity distributions, and high turbulence intensities. This is caused by the air suction due to low-pressure zones on the roof and lateral sides of the building. The detached flow might reattach to the surfaces of the building depending on the upstream surface roughness that determines the turbulence intensity of the incidence flow as well as top and lateral aspect ratios. The downwash flow over the windward façade of the building causes a reverse flow. The reversed flow undercuts the incident wind flow and causes it to be detached from the street level creating a standing vortex near the ground surface upstream of the windward face of the building. This roll-like vortex induces the formation of additional vortices that are smaller in size and are eventually connected to the primary vortex around the lateral sides of the building. This vortex is then stretched around the lateral sides and is extended downwind the building creating a so-called horseshoe-shape vortex [21] (blue region in Figure 4 and Figure 5). The lateral wind flows together with the flow over the top of the building causing the formation of 3D vortices on the leeward side of the building.

The high-rise building's windward façade can direct the high-speed wind at higher elevations down the building's windward façade toward the street level, which is called the downwash effect. The high-rise building creates two longer counter-rotating vortices, thus a longer recirculation region downstream of the building can be noticed. Beyond the buildings, the reattached flow requires some distance to recover the features of incidence wind flow and release all perturbations. This so-called wake region is characterized by velocity deficits, higher turbulence intensities, and smaller-scale eddies compared to the eddies on the windward side. From the L-shape and high-rise building case, it can be seen that the length of wake region on the leeward side of the building increases with an increase in the building's height and length. In the case of cylindrical building with rounded edges, there is no reverse flow zone on the leeward side of the building. The wind flow is less disturbed thus this shape of the building is the most effective in terms of reducing wind loads.

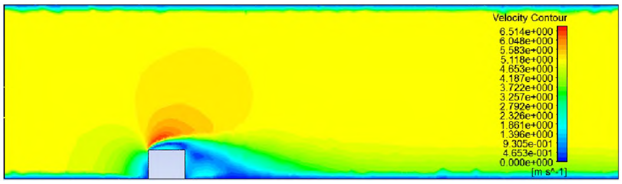

a) cube,

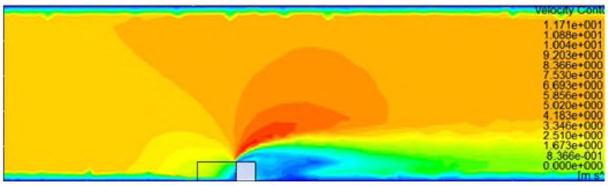

b) L shape

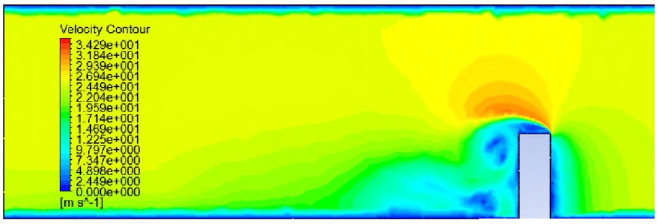

c) high rise

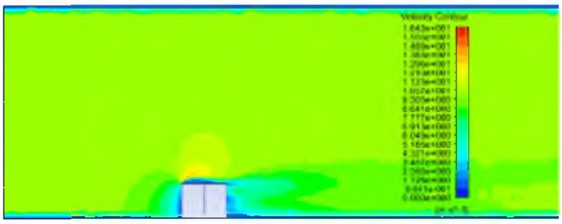

d) cylindrical building

Figure 5. Velocity contours in vertical plane around a) cube, b) L shape, c) high rise, d) cylindrical building

The distribution of turbulence kinetic energy around buildings in the vertical plane is shown in Figure 6. As the height of the building increases, the turbulence kinetic energy also increases. The greatest kinetic energy is above the top face of the building and on the leeward side. The maximum turbulence kinetic energy can be observed near the top of the building while turbulent kinetic energy is lowest in the inflow state. The turbulent kinetic energy increases when wind reaches behind a building due to strong perturbations and a garter velocity gradient. Mean kinetic energy is converted to turbulent kinetic energy due to the formation of eddies that are rotating faster or slower compared to eddies in the mean flow. The kinetic energy is transferred from large to smaller eddies, then to even smaller ones, and so on. On the leeward side, with increased distance from the building, the turbulence kinetic energy decreases, due to dissipation. The turbulence dissipation rate is the velocity at which the mechanical energy of an isotropic small-scale vortex transforms into thermal energy, which greatly influences the diffusion process [22]. With an increase in height, the turbulence dissipation rates vary. The turbulence kinetic energy on the leeward side of the high-rise building is higher compared to other cases, due to the contribution of lateral velocity fluctuation caused by eddies shedding.

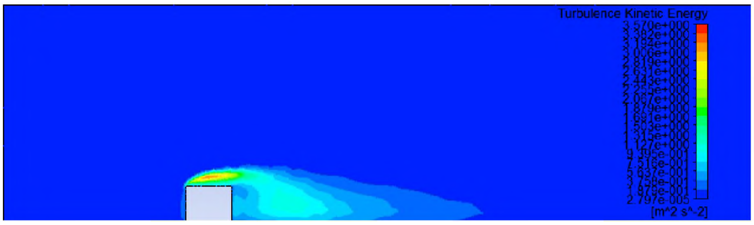

a) cube,

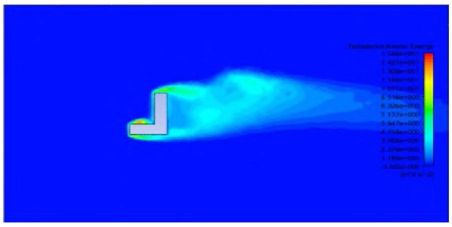

b) L shape

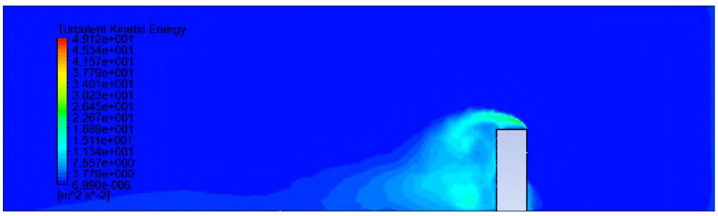

c) high rise

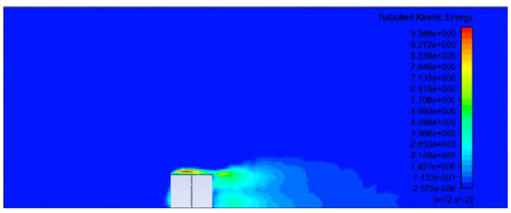

d) cylindrical building

Figure 6. Distribution of turbulence kinetic energy around a) cube, b) L shape, c) high rise, d) cylindrical building

4. Conclusion

It is important to include simulations of wind flow in building design and modern city planning. In this paper, numerical simulations based on Computational Fluid Dynamics (CFD) are performed to study the effect of buildings with different shapes on wind pressure distribution, wind velocity distribution, and distribution of turbulence kinetic energy. The ANSYS Fluent software was used for simulations of wind flow around the isolated cube, high-rise, L-shaped, and cylindrical building. The 3D RANS equations were solved in combination with the standard k-ε model for turbulence modeling while the SIMPLE algorithm was used for pressure-velocity coupling. Analysis of the physics of buildings in terms of shape and height shows a significant correlation with wind flow changes. This is a sign of the direct impact of city physics on wind speed. Different building shape and heights has significant effects on the urban microclimate. Building with a round shape is very effective in withstanding wind stresses, while with the increase in building height, and edges wind flow becomes more disturbed. The results of numerical simulations need to be validated with experimental data from wind tunnel tests. Additional research is needed to study the influence of wind speed which varies with heights of the inlet domain as well as wind direction and wind speed on air temperature in dense built urban areas. Furthermore, the effect of roof slopes on wind flow should be explored.

Nomenclature

Latin symbols

$\bar{v}_i$, $\bar{v}_j$	–	Time-averaged velocity components, [m s-1].
$\bar{F}_i$	–	External forces, [kg m s-2].
$\bar{p}$	–	Time-averaged air presure, in [bar].
v_i', v_j'	–	Fluctuating part of velocity components, [m s-1].
k	–	Turbulence kinetic energy, [m2 s-2].
t	–	Time, [s].
$C_{\varepsilon 1}$	–	Empirical constants.
$C_{\varepsilon 2}$	–	Empirical constants.

Greek symbols

ρ	–	Air density, in [kg m-3].
η	–	Dynamic viscosity, [kg m-1s-1].
ε	–	Turbulent dissipation rate, [m2 s3].
η_t	–	Turbulent viscosity, [m2 s].
σ_k	–	Empirical constants.
σ_ε	–	Empirical constants.

Acknowledgments

The research was funded by the Ministry of Education, Science and Technological Development of the Republic of Serbia (Contract No. 451-03-47/2023-01/200017).

References

[1] Zheng, S., Wang, Y., Zhai, Z., Xue, Y., Duanmu, L., Characteristics of wind flow around a target building with different surrounding building layers predicted by CFD simulation, Building and Environment, 201 (2021), 107962
[2] Liu, S., Pan, W., Zhao, X., Zhang, H., Cheng, X., Long, Z., Chen, Q., Influence of surrounding buildings on wind flow around a building predicted by CFD simulations, Building and Environment, 140 (2018), pp. 1-10
[3] Rajagopalan, P., Lim, K.C., Jamei, E., Urban heat island and wind flow characteristics of a tropical city, Solar Energy, 107 (2014), pp.159-170

[4] Buccolieri, R., Sandberg, M., Sabatino, S.D., City breathability and its link to pollutant concentration distribution within urban-like geometries, Atmospheric Environment, 44 (2010), 15, pp. 1894-1903
[5] Hang, J., Li, Y., Sandberg, M., Buccolieri, R., Di Sabatino, S., The influence of building height variability on pollutant dispersion and pedestrian ventilation in idealized high-rise urban areas, Building Environment, 56 (2012), pp. 346-360
[6] Chang, C-H., Meroney, R.N., Concentration and flow distributions in urban street canyons: wind tunnel and computational data, Journal of Wind Engineering and Industrial Aerodynamics, 91 (2003), 9, pp. 1141-1154
[7] Wen, X., Employment of CFD Simulation on Outdoor Wind Environment for Residential Project Planning and Construction, Science and Technology Innovation Herald, 2010, pp. 113-114
[8] Hunt, J., Fundamental studies of wind flow near buildings, Models and Systems in A rchitecture and Building, LUBFS Conference Proceedings No.2, Publ ished by Constr~ction Press Ltd. (1975), Lunesdale House, Hornby, Lancaster, LA2 BNB
[9] Cao, X., Liu, J., Jiang, N., Chen, Q., Particle image velocimetry measurement of indoor airflow field: A review of the technologies and applications, Energy and Buildings, 69 (2014), pp. 367-380
[10] Jonas Allegrini, J., Viktor Dorer, V., Carmeliet, J., Wind tunnel measurements of buoyant flows in street canyons, Building and Environment, 59 (2013), pp. 315-326
[11] Wang, Y., Zhong, K., He, J., Xu, J., Kang Y., Impacts of wind flow across street-side building gaps on traffic pollutant dispersion at pedestrian level with different block heights, Building and Environment, 246 (2023), 110972
[12] Wu, M., Zhang, G., Wang, L., Liu, X., Wu, Y., Influencing Factors on Airflow and Pollutant Dispersion around Buildings under the Combined Effect of Wind and Buoyancy-A Review, Int. J. Environ. Res. Public Health, 19 (2022), 19, 12895
[13] Blocken B., Stathopoulos, T., van Beeck, J.P.A.J., Pedestrian-level wind conditions around buildings: review of wind-tunnel and cfd techniques and their accuracy for wind comfort assessment, Building and Environment, 100 (2016), pp. 50-81
[14] Oliveira, P.J., Younis, B. A., On the prediction of turbulent flows around full-scale buildings, Journal of Wind Engineering and Industrial Aerodynamics, 86 (2000), 2-3, pp. 203-220
[15] Revuz, J., Hargreaves, D.M., Owen, J.S., On the domain size for the steady-state CFD modelling of a tall building, Wind and Structures, 15 (2012), 4, pp. 313-329
[16] Ansys®, Fluent, ANSYS, Inc.
[17] Blocken, J. Carmeliet, T. Stathopoulos: CFD Evaluation of Wind Speed Conditions in Passages Between Parallel Buildings-Effect of Wall Function Roughness Modifications for the Atmospheric Boundary Layer Flow, Journal of Wind Engineering and Industrial Aerodynamics, 95 (2007), 9-11, pp. 941-962
[18] B. Blocken, T. Stathopoulos, J. Carmeliet: CFD Simulation of the Atmospheric Boundary Layer: Wall Function Problems, Atmospheric Environment, 41 (2007), 2, pp. 238-252
[19] T. H. Shih, W. W. Liou, A. Shabbir, Z. Yang, J. Zhu: A New k-ε Eddy-Viscosity Model for High Reynolds Number Turbulent Flows-Model Development and Validation, Computers and Fluids, 24 (1995), 3, pp. 227-238
[20] Meroney, R., Rafailidis, S., Paageau, M., Dispersion in Idealized Urban Street Canyons, Air Pollution Modeling and its Application, XI, 21, NATO, 1996
[21] Pourteimouri, P., Campmans, G.H.P., Wijnberg, K.M., Hulscher, S.J.M.H., A Numerical Study on the Impact of Building Dimensions on Airflow Patterns and Bed Morphology around Buildings at the Beach, J. Mar. Sci. Eng, 10 (2022), 1, 13
[22] Dongpeng , G., Numerical and Wind Tunnel Simulation Studies of the Flow Field and Pollutant Diffusion around a Building under Neutral and Stable Atmospheric Stratifications, Journal of Applied Meteorology and Climatology, 58 (2019), 11, pp. 2405-2420